Materials Science-Poland, 34(4), 2016, pp. 819-827
http://www.materialsscience.pwr.wroc.pl/
DOI: 10.1515/msp-2016-0119

DE GRUYTER OPEN

Effect of NaOH concentration on optical properties of zinc oxide nanoparticles

VAIBHAV KOUTU*, LOKESH SHASTRI, M. M. MALIK

Nanotechnology Research Laboratory, Department of Physics, Maulana Azad National Institute of Technology, Bhopal (M.P.), India

In the present work, powder zinc oxide samples were prepared by varying NaOH concentration (0.1 M – 0.4 M) using wet-chemical co-precipitation method. As-synthesized ZnO was characterized using X-ray diffraction (XRD), field emission scanning electron microscopy (FESEM), photoluminescence (PL) and Raman spectroscopy. Formation of hexagonal wurtzite structure of the ZnO samples has been revealed from XRD studies. This study further suggests reduction in crystallite size from 40 nm to 23 nm with an increase in NaOH concentration which is confirmed by FESEM. PL and Raman spectroscopy studies of these samples show significant peak shift towards the higher and lower energy respectively, with maximum PL emission between 400 nm and 470 nm region of the visible spectrum. Noticeable inverse relationship between optical properties of ZnO nanoparticles and NaOH concentration may be attributed to the rapid nucleation during the synthesis process. With these remarkable properties, ZnO nanoparticles may find applications in nanoelectronic devices, sensors, nanomedicine, GATE dielectrics, photovoltaic devices, etc.

Keywords: *NaOH concentration; ZnO nanoparticles; peak shift*

1. Introduction

ZnO is a direct bandgap wurtzite semiconductor having bandgap of 3.37 eV and large exciton binding energy (∼60 meV) at room temperature [1]. With the advent of nanotechnology, zinc oxide (ZnO) has been a center of attraction. The reasons for the keen interest in ZnO were attributed to its excellent properties such as easy synthesis, tunable bandgap [2], controllable shape and size, low cost of production and non-toxicity [2]. Most important amongst all are its remarkable optical properties which allow ZnO to emit light in the entire visible region (from violet to red) [3]. Various workers [1, 3, 4] suggested that the presence of large number of extrinsic and intrinsic defects and complexes in the ZnO structure acts as emission centers. Depending upon the level and positions of these centers, ZnO is able to emit light in various colors such as violet, blue, green, yellow, orange and red [3, 4]. Because of these remarkable and peculiar properties, ZnO has a wide range of applications in the areas ranging from photovoltaic [5] to photocatalyst [6, 7], from electronics [2] to medical sciences [2, 7] and from cosmetics [5] to antibacterial applications [6].

Intensive studies have been done on various factors, such as precursor concentrations [8, 9], temperature [10, 11], duration [12], surfactant concentration [7], dopant concentration [6], solvent medium [13], pH of reaction mixture [14] and source of light during synthesis [15], which individually and collectively affect the shape, size and optical properties of ZnO. Various researchers [16–18] suggested that NaOH concentration plays a vital role in determining the morphology, size and optical bandgap of obtained nanostructures. The survey of many significant reports [8, 17, 18] reveals that the size of the nanostructures is directly proportional to the NaOH concentration where the particle size increases accordingly. This phenomenon is explained in terms of Ostwald ripening [2, 5]. According to this, under synthesis conditions, tiny crystallites nucleate first and then they

*E-mail: 123105005_ aibhav@manit.ac.in

agglomerate into larger crystallites due to the energy difference between large and smaller particles of higher solubility based on Gibbs-Thomson law [19]. This in turn leads to a subsequent increase in the number of energy states of the material causing narrowing of the separation between the highest occupied valence band and the lowest occupied conduction band, which in turn, reduces the band gap of the material [8].

In the present work, wet chemical co-precipitation method [2, 4, 17, 20, 21] has been opted for the synthesis of ZnO samples and their optical properties were studied at different NaOH concentrations. High purity ZnO nanospheres with decreasing diameter were obtained as the NaOH concentration increased. There was reduction in size of the as-prepared ZnO nanostructures which may be due to fast nucleation during the synthesis process.

2. Experimental

Zinc acetate dihydrate ($Zn(CH_3COO)_2{\cdot}2H_2O$) and sodium hydroxide (NaOH) of 99.95 % purity were purchased from Sigma-Aldrich and used without further purification. 100 mL of double-distilled water was measured in a sealed flask fitted with a burette. To this flask, 0.1 M of $Zn(CH_3COO)_2{\cdot}2H_2O$ was added and the solution was stirred at 600 rpm at 90 °C. 100 mL of equimolar sodium hydroxide (keeping $Zn(CH_3COO)_2{\cdot}2H_2O$:NaOH molar ratio at 1:1) was added to this freshly prepared zinc solution and the mixture was stirred for 1 hour at the same temperature. The mixture was then refluxed at 90 °C for 1 hour. The final mixture was cooled at room temperature for 24 hours to get precipitation. The precipitate obtained after cooling was then washed with methanol. The process of washing was repeated for several times to remove the organic impurities and other unreacted compounds from the obtained product. The final precipitate was then dried in vacuum at room temperature to obtain the final product (zinc oxide).

The same procedure was followed to prepare zinc oxide using 0.2 M, 0.3 M and 0.4 M NaOH concentrations while keeping $Zn(CH_3COO)_2{\cdot}2H_2O$ concentration fixed at 0.1 M. All the samples were finely grinded using an agate mortar and a pestle and the powders were then kept in air-tight vials. The final ZnO powders (C1–C4) are listed in Table 1. The complete set of experiment was repeated twice to check and confirm the variation of particle size of the samples with respect to NaOH concentration.

The samples were characterized using X-ray diffractometer Rigaku MiniFlex II with 1.54 Å Cu-Kα radiation for confirmation of the crystal structure and purity of the as-prepared products. X-ray diffraction analysis was done in the range 20°– 80° (2θ) at the scan rate of 3°/min. Morphology of the samples was studied by Nova NanoSEM field emission scanning electron microscope. Emission study was carried out by Hitachi F-7000 photoluminescence spectrophotometer and the vibrational properties of the nanoparticles were studied by INVIA-Reflex Raman spectrophotometer, Renshaw Meterology, India.

3. Results

3.1. X-ray diffraction (XRD) analysis

Fig. 1a shows typical XRD patterns of the as-prepared samples obtained at different NaOH concentrations by wet-chemical method. All the peaks in the obtained patterns are well matched with the JCPDS file #79-0206 of the standard ZnO which can be indexed as corresponding to the reflection of hexagonal wurtzite ZnO. No characteristic peaks of impurity phases were observed. Cell parameters were calculated from the diffraction pattern and the obtained values: a = 3.154 Å and c = 5.023 Å were slightly smaller than those of the standard JCPDS #79-0206 cell parameters, a = 3.249 Å and c = 5.206 Å.

3.2. Field emission scanning electron microscope (FE-SEM) analysis

Field emission scanning electron microscopy (FE-SEM) images, shown in Fig. 2, show the morphology of the as-prepared ZnO nanoparticles (C1–C4). All the samples were analyzed at 10 kV accelerating voltage.

Table 1. List of final ZnO samples (C1–C4) obtained at different NaOH concentrations.

Sample	Precursor concentration		Molar	Reaction	Heating
	Zinc acetate	NaOH	ratio	temperature	time
C1	0.1M	0.1M	1:1	90 °C	2 h
C2	0.1M	0.2M	1:2	90 °C	2 h
C3	0.1M	0.3M	1:3	90 °C	2 h
C4	0.1M	0.4M	1:4	90 °C	2 h

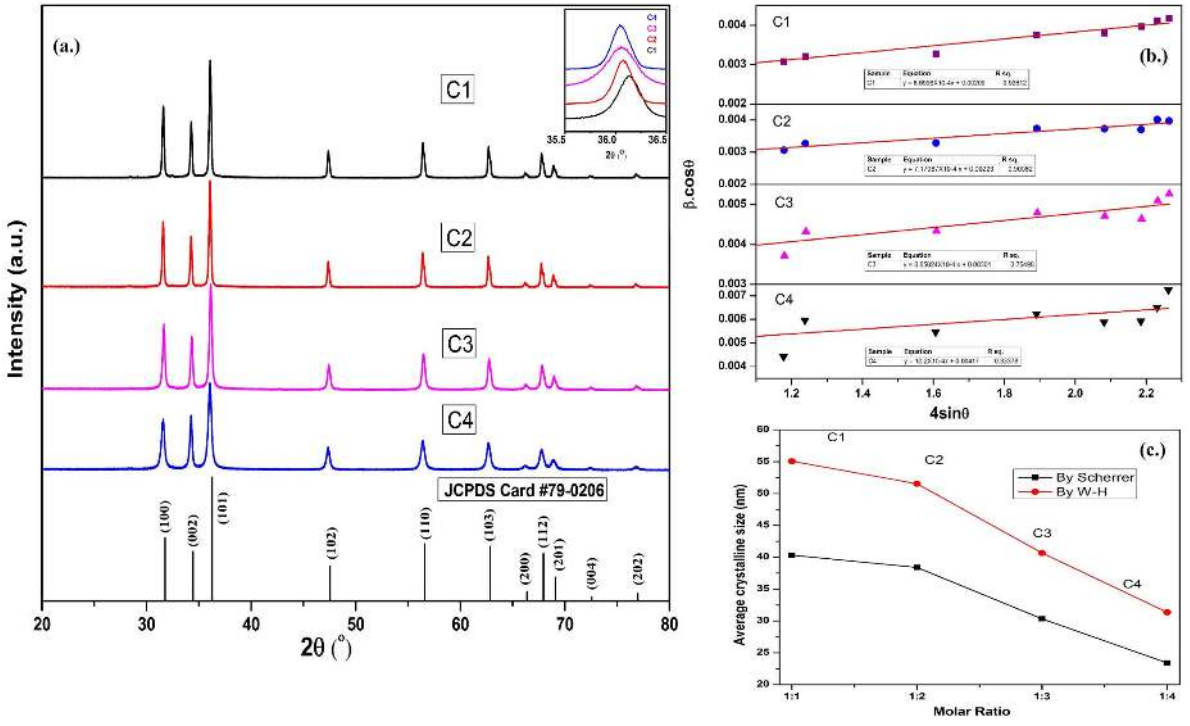

Fig. 1. (a) XRD pattern of as-prepared ZnO samples prepared at different NaOH concentrations (the inset shows variation of peak width and position of (1 0 1) peak with respect to NaOH concentration), (b) Uniform Deformation Model (UDM) of as-prepared ZnO nanoparticles using Williamson-Hall analysis (Tables show linear fit equation of the corresponding sample), (c) variation of crystallite size of as-prepared ZnO nanoparticles with respect to molar ratio.

3.3. Photoluminescence (PL) analysis

Optical emission of the above samples was studied by photoluminescence spectroscopy. The samples were excited at 320 nm excitation wavelength and the emission spectrum of each sample was plotted, as shown in Fig. 3.

3.4. Raman spectroscopy

In order to study the effect of reaction temperature on the vibrational properties of as-prepared ZnO samples, their room temperature Raman spectra were measured using 633 nm laser source at 10 mW power. Fig. 4 shows the Raman spectra of all the as-prepared ZnO samples.

4. Discussion

4.1. X-ray diffraction (XRD) analysis

Comparing the sample diffraction data (Fig. 1a) with the standard JCPDS #79-0206, slight shift

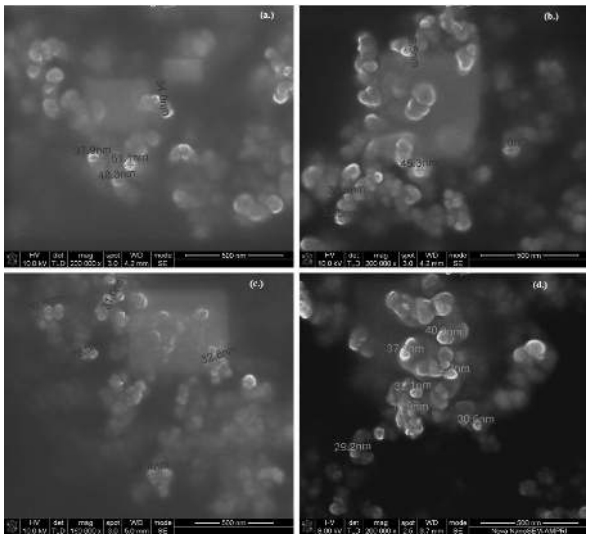

Fig. 2. SEM images showing morphology of the ZnO samples prepared at different temperatures: (a) C1, (b) C2, (c) C3, and (d) C4.

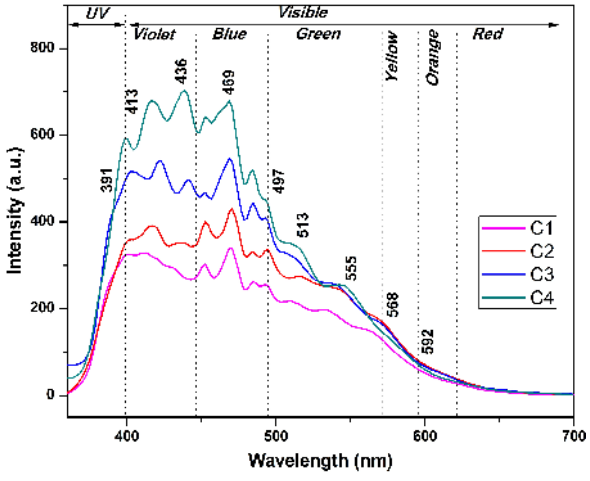

Fig. 3. Photoluminescence spectra of as-prepared ZnO nanoparticles excited at 320 nm exciton absorption wavelength.

towards lower Bragg angles is observed which represents the presence of uniform strain in the crystallites of the as-prepared samples [24]. The diffraction peaks are also broadened which represents smaller crystallite size of the material. Small variation in the intensity and broadening of peaks represents the rearrangement of crystal plane according to synthesis conditions [23]. Also reduction of the values of cell parameters: a and c indicates

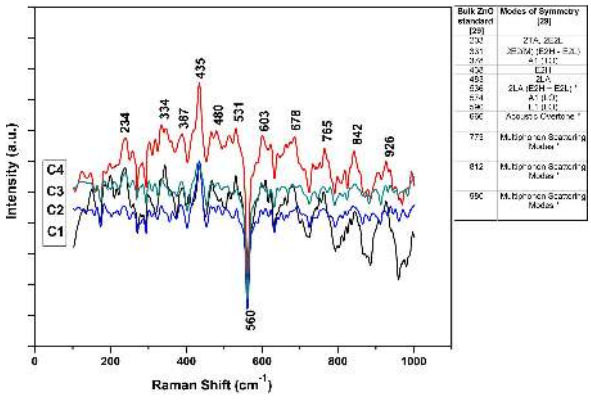

Fig. 4. Raman spectra of as-prepared ZnO nanoparticles (the inset shows the Raman shifts for standard ZnO).

the presence of some stress or strain in the crystal lattice of the samples [22, 23]. The strain observed in the samples can be explained by the Uniform Deformation Model (UDM) using Williamson-Hall (W-H) plot [22, 24] which claims that the diffraction line broadening is due to strain (ϵ) effect and reduction in crystallite size. The UDM equation was calculated by using the diffraction peak broadening and is given by [22, 24]:

$$\beta \cos\theta = k\lambda/d + 4\varepsilon \sin\theta \qquad (1)$$

This equation represents the Uniform Deformation Model (UDM) which assumes that the strain is uniform in all crystallographic directions [22, 24]. The amount of strain was calculated by plotting a graph $\beta\cos\theta$ versus $4\sin\theta$ shown in Fig. 1b. The two main properties extracted from the plot are the crystallite size and the associated lattice strain.

From the linear fit of the data (Fig. 1b), the crystallite size (d) is calculated from the y-intercept, and the microstrain (ϵ) is obtained from the slope of the linear fit [22, 24]. The strain may be either compressive or tensile. The strain (ϵ_{zz}) in the samples along c-axis can be calculated using equation [25] given by:

$$\varepsilon_{zz} = (c - c_o) \cdot 100/c_o \qquad (2)$$

where c_o is the unstrained lattice parameter and c is the lattice parameter calculated from the XRD data. The value of the strain calculated from equation 2

was −3.515. Negative value accounts for the compressive strain [25] and it is also confirmed by the values of microstrain ϵ calculated from the W-H plot of the samples (Table 2). The values of average crystallite size calculated by both UDM method and Scherrer method, and strain for all the samples are listed in Table 2.

From Table 2, it is observed that the crystallite size of the as-prepared ZnO samples is reduced with the increase in the NaOH concentration, which is well supported by the increase in the values of strain in the samples with respect to the NaOH concentration. Various researchers [22–24] have reported that the strain in the samples is inversely proportional to the crystallite size, and this is clearly observed in the above results also. The strain may be caused by the change in the bond-length due to a change in the values of lattice constants (a and c) [23] and due to charge-carrier gradient within the crystal structure, resulting in overall shrinkage of the crystallite size.

Fig. 1c shows the variation in the crystallite size of the as-prepared ZnO nanoparticles (obtained by Scherrer analysis and W-H analysis) with respect to the NaOH concentration.

From the crystallite size vs. molar ratio plot (Fig. 1c), it is observed that there is a small variation in the values of the crystallite size obtained from both the methods. This variation is caused by the difference in averaging the particle size distribution [22]. The curves show a linear and systematic reduction in the crystallite size with an increase in NaOH concentration from 0.1 M (sample C1) to 0.2 M (sample C2) and a sudden drop in the crystallite size on further increasing NaOH concentration to 0.3 M (sample C3) and 0.4 M (sample C4). There may be two possible phenomena responsible for obtaining smaller crystallite size: (a) supersaturation, (b) NaOH reaction within the solution mixture.

Supersaturation is critical because it is a driving force for crystal nucleation and growth. At low supersaturation, crystals can grow faster than they nucleate, which results in a larger crystal size while at higher supersaturation, crystal nucleation dominates crystal growth, ultimately resulting in smaller crystals [26]. The obtained results are in fair agreement with the observation that by increasing the level of supersaturation, the crystallite size is reduced.

During the synthesis, gradual adding of NaOH to the zinc acetate solution may have caused sudden temperature gradient resulting in fast nucleation. It has been suggested that Na^+ is attracted by the OH^- around the nanocrystal and forms a virtual capping layer, thus, inhibiting the nanocrystal growth [2]. This is explained by the help of following equations:

$$Zn^{2+} + 2OH^- \longleftrightarrow Zn(OH)_2 \tag{3}$$

$$Zn(OH)_2 + 2OH^- \longleftrightarrow [Zn(OH)_4]^{2-} \tag{4}$$

$$[Zn(OH)_4]^{2-} \longleftrightarrow ZnO_2^{2-} + 2H_2O \tag{5}$$

$$ZnO_2^{2-} + H_2O \longleftrightarrow ZnO + 2OH^- \tag{6}$$

$$ZnO + OH^- \longleftrightarrow ZnOOH^- \tag{7}$$

$$ZnOOH^- + Na^+ \longleftrightarrow ZnOOH - Na \tag{8}$$

In equation 4, the product is not necessarily $Zn(OH)_4^{2-}$, but could also be in the form of $Zn(OH)^+$, $Zn(OH)_2$, or $Zn(OH)^{3-}$, depending on the parameters, such as the concentration of Zn^{2+} and OH^- ions [2]. Depending upon concentrations of Na^+ and OH^- ions, the size of nanocrystals varies which could be observed in the obtained results for the samples. This reduction in size may have induced development of strain in the crystal lattice which would have led to an increase in the number of intrinsic and/or extrinsic defects in the particles. These observations could be easily seen in the FE-SEM images of the as-prepared samples also.

Table 2. Calculated values of average crystallite size and strain for the as-prepared ZnO nanoparticles by UDM (W-H plot) and Scherrer formula.

Sample	Average crystallite size		Strain (ϵ)
	UDM (W-H plot)	Scherrer formula	
C1	55 nm	40 nm	2.133×10^{-3}
C2	51 nm	38 nm	2.163×10^{-3}
C3	40 nm	30 nm	2.743×10^{-3}
C4	31 nm	23 nm	3.597×10^{-3}

Table 3. Average diameter of as-prepared ZnO nanoparticles obtained from field emission scanning electron microscope images.

Sample	Molar ratio	Average particle size
C1	1:1	60 nm
C2	1:2	58 nm
C3	1:3	52 nm
C4	1:4	50 nm

4.2. Field emission scanning electron microscope (FE-SEM) analysis

FESEM images show the presence of homogenous, well-dispersed particles having well-defined grain boundaries. Particle growth in a wet-chemical process could be explained by the phenomenon of nucleation and then aggregation [2]. Actually, the rate of particle growth is governed by the concentration of the precursors and their reactivity. In the present work, crystal nucleation is dominant because of higher supersaturation of NaOH, resulting in rapid conversion of Zn^{2+} ions into $[Zn(OH)_4]^{2-}$ complexes with relatively low aggregation, which leads to smaller particle size with spherical shape [2, 26] having the average diameter of 60 nm for sample C1 and 50 nm for sample C4. The FESEM images show reduction in the diameter of the ZnO nanoparticles which is in accordance with the XRD peak width (FWHM) analysis and the crystallite size calculations of the samples (Table 2). Table 3 shows the average diameter of as-prepared samples obtained from the field emission scanning electron microscope images.

4.3. Photoluminescence (PL) analysis

Fig. 3 shows emission spectra of the as-prepared ZnO nanoparticles excited at 320 nm. Various researchers [3, 21, 22] suggest that the PL spectrum of ZnO generally consists of two emission bands: one in the UV region (near 370 nm to 400 nm) and a broad band in the visible region (400 nm to 700 nm) of the spectrum. Depending upon the intensity and width of the peaks in the corresponding band, one can infer the structure of the material. For instance, in case of nanorods and nanotubes, the PL spectrum mainly consists of a strong and sharp UV emission band and a relatively weak defect (visible) emission peak [2, 21, 27], while in case of quantum dots and spherical nanoparticles, PL spectrum shows a weak UV emission band and a broad visible emission band covering almost entire visible region [3, 22]. These studies and the emission spectra of the as-prepared ZnO samples clearly show that the as-prepared ZnO samples are spherical in shape having nanodimensions which is also confirmed by the FESEM images of the samples.

According to the available reports [3, 21, 22, 27], a defect free perfect crystal of ZnO has a single emission peak in the visible region while an increase in the number of emission peaks indicates the presence of defect levels in the material. The position of the peaks provides information about the depth and type of defects in the material [3].

In the emission spectra (Fig. 3), a small peak centred between 380 nm to 390 nm (UV region) is observed for all the samples while multiple peaks are observed from violet to green region

of the spectrum. The major emission peaks in the visible region are centred between 400 nm to 445 nm (violet region), 445 nm to 495 nm (blue region) and 495 nm to 565 nm (green region). The study of the PL graph also shows that with the increase in NaOH concentration emission peaks around 568 nm (yellow region) and 592 nm (orange-red region) appear for samples C3 and C4 but are absent in samples C1 and C2. Moreover, most of the prominent emission peaks show a shift towards higher energy (blue shift) with an increase in NaOH concentration.

These yellow and orange-red emissions are caused by oxygen interstitials and oxygen interstitials-zinc vacancies complexes respectively [28]. It may be inferred that high O^-/O^{2-} ion concentration increases intrinsic strain in the lattice of the sample due to trapping of oxygen ions from the reaction solution into the interstitials which causes transitions from conduction bottom to the oxygen interstitial site emitting yellow emissions around 2.2 eV [22, 28]. Moreover, it could have also caused zinc vacancies in the crystal thus resulting in the formation of zinc vacancies complexes causing transitions from vacant zinc sites to interstitial oxygen sites [28]. Most prominent emission bands observed from the emission spectra are in the blue and green region which may be due to lattice defects developed as a result of compressive strain produced at the intrinsic crystal lattice [21, 28]. This leads to the formation of oxygen and zinc vacancies and interstitials simultaneously, which causes transition of energy from conduction band or zinc interstitials to the vacant zinc sites [21, 22, 28] resulting in blue emission, while the same originating from deep levels causes green emissions. The UV, violet and green emission bands, also visible in the spectra, are caused by their corresponding defect sites as reported by various researchers [3, 21, 22, 27].

Further, it is observed that the prominent emission peaks show blue shift with the increase in NaOH concentration. This peak shift may be attributed to the development of strain in the crystal structure which can be easily observed from the Uniform Deformation Model (UDM) explained in Fig. 1b. Comparing the values of strain from UDM analysis, it can be inferred that increasing the supersaturation (NaOH concentration) results in increment in the values of compressive strain, which in turn increases the intrinsic defects in the material as it is clearly observed in the corresponding emission spectra. This strain may have affected the bond length as well as the bond angle of the lattice [22] which could have resulted in the development of various defects in the crystal structure like oxygen vacancy (V_O), zinc vacancy (V_{Zn}), oxygen interstitial (Oi), zinc interstitial (Zni), oxygen anti-site (O_{Zn}), and zinc anti-site (Zn_O) [3, 21, 22, 27]. The position of the emission peaks varies with the NaOH concentration and could be related to the depth of the level of defects in the crystal structure of the sample causing Deep Level Emissions (DLE) [28]. Although the exact mechanism of the deep level emissions is still unclear, it could be inferred that these deep levels create intermediate states in the band gap of the material [3].

The PL spectra show that for UV exciton wavelengths, the ZnO samples show high emission intensity in broad visible region, hence ZnO becomes a promising material for applications in the field of UV detectors and sensors as well as photoelectric devices.

4.4. Raman spectroscopy

Fig. 4 shows room temperature Raman spectra of the as-prepared ZnO samples measured using 633 nm laser source at 10 mW power. Various researchers [30–32] reported that wurtzite ZnO belongs to the space group C_{6v}^4 with two formula units per primitive cell where all atoms occupy C_{3v} sites. Also, it is well known that ZnO has eight sets of characteristic optical phonon modes at the center of Brillouin zone (Γ-point), which according to group theory [21, 27, 29] is predicted as:

$$\Gamma_{opt} = 1A_1 + 2B_1 + 1E_1 + 2E_2 \qquad (9)$$

where A_1 and E_1 are two polar phonon modes, each comprising of longitudinal optical (LO) and transverse optical (TO) components, which are both Raman and IR active; E_2 is non-polar and only Raman

active with two frequency modes: E_2 low (E_{2L}) for Zn sublattice and E_2 high (E_{2H}) for oxygen sublattice while B_1 modes are Raman inactive [30–32]. Strong E_{2H} mode is characteristic of wurtzite lattice and shows good crystallinity [30].

From Fig. 4, one can find that with an increase in NaOH concentration there is a significant red shift (lower energy) in the peaks centered around 435 cm^{-1} for E_{2H} mode, 531 cm^{-1} for 2LA $\{E_{2H}+E_{2L}\}$ mode, 560 cm^{-1} for A_1(LO) mode and 765 cm^{-1} and 926 cm^{-1} for multiphoton scattering [29, 30, 32] as well as blue shift towards higher energy in the Raman peaks centered around 334 cm^{-1} for $2E_2$(M) $\{E_{2H}-E_{2L}\}$ mode, 387 cm^{-1} for A_1 (TO) mode, 480 cm^{-1} for 2LA mode, 603 cm^{-1} for E_1(LO) mode, 678 cm^{-1} for acoustic overtone vibration mode. It also reveals that the samples have nanodimensions [30, 32]. The peaks around 234 cm^{-1} may be attributed to the $2E_{2L}$ second order phonon mode which may have arose due to presence of zinc sublattice [29, 32].

According to the available reports [29–32] for bulk ZnO, A_1 (LO) phonon mode is commonly assigned to the oxygen vacancies, zinc interstitials or defect complexes containing oxygen vacancy and zinc interstitial in ZnO. Strong multiphonon scattering reveals quantum confinement effect in the material and the optical phonon confinement resulting in phonon frequency shift of few cm^{-1} in the sample [32]. These two phenomena are observed in the Raman spectra of the as-prepared nanoparticles also.

Out of the four fundamental characteristic peaks for wurtzite hexagonal ZnO, two dominant peaks at 435 cm^{-1} (corresponding to E_{2H} phonon modes) and other at 560 cm^{-1} (for A_1(LO) mode) are red shifted as compared to the corresponding peaks of standard ZnO. Hence, the effect of blue phonon shift could be ignored. Moreover, there is asymmetric broadening in the E_{2H} mode ($\sim$435 cm^{-1}) of the samples. This broadening of the spectra, asymmetric line shape and strong red shift of E_{2H} mode towards lower energy may be attributed to the optical phonon confinement [27, 30–32]. Spatial confinement by the nanostructure boundaries and phonon localization of defects [32] may be responsible for the observed peak shifts in the corresponding Raman spectra with the rise in NaOH concentration. It may also be attributed to the presence of surface defects [32] or deep level defects [29, 31] in the samples. Comparing with the emission spectra (Fig. 3), one can infer that the deep level defects may have caused the red shift in the Raman peaks [29, 31]. From the study of X-ray diffraction patterns and emission properties studies, it has been shown that these defects are attributed to the compressive strain in the crystals which was found dependent on the NaOH concentration. The obtained experimental results are in fair agreement with the Fonoberov and Balandin theory of optical phonons [31, 32], according to which the asymmetry of wurtzite crystal lattice leads to the quantum dot shape-dependent splitting of the frequencies of polar optical phonons in a series of discrete frequencies.

The obtained results agree with the phenomenon of optical phonons in as-prepared ZnO nanoparticles and could be well-harnessed in the applications of optoelectronic and photoelectronic devices.

5. Conclusions

The above results indicate inverse effect of NaOH concentration on particle size as well as on the optical properties of ZnO nanoparticles. The reduced dimensional spherical particles have uniform shape distribution and show broad and intense emission in the visible region when excited by a UV exciton wavelength. The photoluminescence characteristics of the ZnO samples could be improved by using silver, gold or other metallic ions as dopants, which could additionally improve the emission as well as the electrical and thermal properties also. Thus, the above study reveals that these nanoparticles with inverse effect of NaOH, particularly on their size, may find applications in nanoelectronic devices, UV sensors and detectors, photovoltaic devices, GATE dielectrics, bio-medical engineering etc.

Acknowledgements

The authors would like to thank MHRD Government of India and Director MANIT Bhopal for providing scholarship

to one of the authors (Vaibhav Koutu). Also, the authors would like to acknowledge Dr. O. P. Modi, Chief Scientist and Mr. Muhamad Shafeeq, Technical Assistant, Materials Characterization Laboratory, AMPRI Bhopal for X-ray diffraction characterization and Field Emission Scanning Electron Micrography of the samples, and Mr. Pranay Dubey, SIC, Dr. H. S. Gaur University Sagar for Raman analysis of the samples.

References

[1] ZHANG X., QIN J., XUE Y., YU P., ZHANG B., WANG L., LIU R., *Sci. Rep.-UK*, 4 (2014), 4596.
[2] XU S., WANG Z.L., *Nano Res.*, 4 (2011), 1013.
[3] WILLANDER M., NUR O., SADAF J.R., QADIR M.I., ZAMAN S., ZAINELABDIN A., BANO N., HUSSAIN I., *Materials*, 3 (2010), 2643.
[4] KOŁODZIEJCZAK-RADZIMSKA A., JESIONOWSKI T., *Materials*, 7 (2014), 2833.
[5] UMAR A., HAHN Y.B., *ZnO Nanoparticles: Growth, Properties, and Applications*, in: UMAR A., HAHN Y.B. (Eds.), *Metal Oxide Nanostructures and Their Applications*, American Scientific Publishers, California, 2010, p. 1.
[6] PODPORSKA-CARROLL J., MYLES A., QUILTY B., MCCORMACK D.E., FAGAN R., HINDER S.J., DIONYSIOU D.D., PILLAI S.C., *J. Hazard. Mater.*, (2015).
[7] KUNDU S., *Colloid. Surface. A*, 446 (2014), 199.
[8] CHAND P., GAUR A., KUMAR A., GAUR U.K., *Appl. Surf. Sci.*, 356 (2015), 438.
[9] JYOTI M., VIJAY D., RADHA S., *IJSRP*, 3 (2013), 1.
[10] NARAYANAN G.N., GANESH R.S., KARTHIGEYAN A., *Thin Solid Films*, 598 (2016), 39.
[11] KUMAR S.S., VENKATESWARLU P., RAO V.R., RAO G.N., *Int. Nano Lett.*, 3 (2013), 1.
[12] PHOLNAK C., CHITNARONG S., SUMETHA S., DAVID J.H., *Mater. Res.*, 17 (2014), 405.
[13] BAGABAS A., ALSHAMMARI A., ABOUD M.FA, KOSSLICK H., *Nanoscale Res. Lett.*, 8 (2013) 1.
[14] WAHAB R., ANSARI S.G., KIM Y.S., SONG M., SHIN H.S., *Appl. Surf. Sci.*, 255 (2009), 4891.
[15] PRADHAN P., JUAN C.A., MONSERRAT B., *Int. J. Photoenergy*, 2012 (2012), 1.
[16] SONIA S., JAYRAM N.D., SURESH KUMAR P., MANGALARAJ D., PONPANDIAN N., VISWANATHAN C., *Superlattice. Microst.*, 66 (2014), 1.
[17] MOAZZEN M.A.M., SEYED M.B., FARSHAD T., *Appl. Nanosci.*, 3 (2013), 295.
[18] ANANDHAVELU S., THAMBIDURAI S., *Mater. Chem. Phys.*, 131 (2011), 449.
[19] POLSONGKRAM D., CHAMNINOK P., PUKIRD S., CHOW L., LUPAN O., CHAI G., KHALLAF H., PARK S., SCHULTE A., *Physica B*, 403 (2008), 3713.
[20] KAHOULI M., BARHOUMI A., BOUZID A., AL-HAJRY A., GUERMAZI S., *Superlattice. Microst.*, 85 (2015), 7.
[21] SAMANTA P.K., PATRA S.K., GHOSH A., CHAUDHURI P.R., *Int. J. Nanosci. Nanotechno.*, 1 (2009), 81.
[22] BINDU P., THOMAS S., *J. Theor. Appl. Phys.*, 8 (2014), 123.
[23] HASSAN M.M., KHAN W., AZAM A., NAQVI A.H., *J. Lumin.*, 145 (2014), 160.
[24] ZAK A.K., MAJID W.H.A., ABRISHAMI M.E., YOUSEFI R., *Solid State Sci.*, 13 (2011), 251.
[25] NAVIN K., KURCHANIA R., *Appl. Phys. A-Mater.*, 121 (2015), 1155.
[26] MULLIN J.W., *Crystallization*, Elsevier, London, 2001.
[27] ZHANG R., YIN P.G., WANG N., GUO L., *Solid State Sci.*, 11 (2009), 865.
[28] ALIM K.A., FONOBEROV V.A., BALANDIN, A.A., *Appl. Phys. Lett.*, 86 (2005), 53103.
[29] ARTUS L., CUSCO R., ALARCON-LLADO E., GONZALEZ-DIAZ G., MARTIL I., JIMENEZ J., WANG B., CALLAHAN M., *Appl. Phys. Lett.*, 90 (2007), 181911.
[30] CAO W., DU W., *J. Lumin.*, 124 (2007), 260.
[31] ZEFERINO R.S., FLORES M.B., PAL U., *J. Appl. Phys.*, 109 (2011), 014308.
[32] FONOBEROV V.A., BALANDIN A.A., *Properties of GaN and ZnO quantum dots*, in: BALANDIN A.A., WANG K.L. (Eds.), *Handbook of Semiconductor Nanostructures and Nanodevices*, American Scientific Publishers, Los Angeles, 2006, p. 119.

Received 2016-04-13
Accepted 2016-10-18